

Asymmetric Transfer Hydrogenation of Prochiral Ketones Catalyzed by Ru(II)-NH-propyl-(1R,2S)-(+)-cis-1-amino-2-indanol Complexes Immobilized on SBA-15

Aneesh Mathew¹, Surendran Parambadath^{2*}

¹Department of Basic Science, Government Engineering College, Painavu, Idukki, Kerala, India, ²Department of Chemistry, Sree Neelakanta Government Sanskrit College (Affiliated to University of Calicut), Pattambi, Palakkad, Kerala, India

ABSTRACT

NH-propyl-(1R,2S)-(+)-cis-1-amino-2-indanol (Pr-AIL) was immobilized on SBA-15 by a step by step post-synthesis modification method. (3-chloropropyl) trimethoxysilane (3-CPTMS) was functionalized on SBA-15 further the silanol groups were passivated by dimethoxydimethylsilane [Pr-SBA-15]. There after (1R,2S)-(+)-cis-1-amino-2-indanol (1R,2S-AIL) was anchored over functionalized SBA-15 [PrAIL-SBA-15]. The heterogeneous catalysts were synthesized by complexation of PrAIL-SBA-15 using $[\text{RuCl}_2(\text{benzene})]_2$ and $[\text{RuCl}_2(p\text{-cymene})]_2$ in 2-propanol at reflux condition and were designated as Ru-1 and Ru-2, respectively. The synthesized heterogeneous materials were characterized by small angle X-ray diffraction spectroscopy (SAXS), scanning electron microscopy (SEM), transmission electron microscopy (TEM), N₂ adsorption-desorption isotherms, Fourier-transform Infrared (FT-IR) spectroscopy, ²⁹Si magic angle spinning (MAS) and ¹³C cross-polarization magic angle spinning (CP-MAS) NMR spectroscopies, intensively coupled plasma atomic emission spectroscopy (ICP-AES), diffuse reflectance UV-Vis spectroscopy, and X-ray photoelectron spectroscopy (XPS). Further, the synthesized and characterized heterogeneous materials were successfully applied in the asymmetric transfer hydrogenation (ATH) reaction of simple prochiral ketones. The reactions were exhibited high catalytic activities and excellent enantioselectivities for most of the simple aromatic ketones. The factors such as time, temperature, amount of solvent, and base also were studied in detail by keeping acetophenone as a model molecule and Ru-1 as a catalyst. In particular, these heterogeneous catalysts could be readily recovered by simple filtration and reused in multiple consecutive catalytic runs without losing the enantiomeric excess (*ee*) values.

Key words: Mesoporous molecular sieve, SBA-15, Chiral amino alcohols, Asymmetric transfer hydrogenation, Prochiral ketones.

1. INTRODUCTION

Enantiomerically pure secondary alcohols are among the most valuable key intermediates for the manufacture of pharmaceuticals and advanced materials. The simplest and most powerful way to produce chiral alcohols is the asymmetric hydrogenation and transfer hydrogenation of ketones [1,2]. Among the enantioselective transformations, the clean asymmetric hydrogenation of ketones is a reaction of particular importance to the pharmaceutical industry due to the mild reaction conditions, operational simplicity, low fractional yields of side products, and high product yields in high enantiomeric purity. Among the great progress achieved in this area, the most significant to date is perhaps the discovery of the catalyst consisting of a ruthenium(II) complex with (*R,R*)- or (*S,S*)-*N*-(*p*-toluenesulfonyl)-1,2-diphenylethylenediamine (TsDPEN) reported by Noyori *et al.* [3]. Afterward, J. M. J. Williams developed a water-soluble analogous of Noyori's catalyst to make it more eco-friendly and has observed that it is functioning as effective as Noyori's catalyst [4]. However, the homogenous nature of many of such type complexes limits their wide utility in industrial processes. Several methods have been proposed for the heterogenization of chiral catalysts. Immobilization to the surface of silica or a polymer has been more attracted in these attempts because of the comparable activity and enantioselectivity with its homogenous analogous. For silica support simple filtration or centrifugation is enough to separate the highly precious metal catalyst and for polymer

the recycling by re-precipitation by the addition of suitable solvents to the reaction mixture after use [5]. Covalent anchoring of chiral catalysts to supports such as zeolite, layered clays, or silica has been shown to give highly effective enantioselective catalysts. Matrix isolation of chiral catalysts in microporous solids has been limited until recently by the difficulty of obtaining materials with suitable pore characteristics. Mesoporous materials can offer many attractive features for the heterogenization of homogeneous complexes including uniform large pore size, high surface area, insolubility in organic solvents, and inert to many chemical substrates.

Covalently anchored heterogeneous analogous of Noyori's catalyst was introduced by Tu *et al.* [6,7] on amorphous silica gel, mesoporous MCM-41, and SBA-15 for asymmetric transfer hydrogenation of various

*Corresponding author:

Surendran Parambadath

E-mail: sr.parambadath@yahoo.com

ISSN NO: 2320-0898 (p); 2320-0928 (e)

DOI: 10.22607/IJACS.2024.1204002

Received: 22nd November, 2024;

Revised: 28th December, 2024;

Accepted: 29th December, 2024

Published: 30th December, 2024

ketones in water, which showed superior enantioselectivities and very high reactivities toward a number of substrates in presence or absence of an additive [8]. The MCM-41-supported chiral *N*-sulfonyldiamine was used as an efficient heterogeneous chiral ligand in the asymmetric transfer hydrogenation of ketone. Immobilized chiral Ru-TsCHDA catalyst onto SBA-15 has exhibited remarkably high catalytic activities and excellent enantioselectivities [9]. Fluorescence-marked core-shell structured nanocatalyst was found to be good catalytic efficiency for asymmetric transfer hydrogenation of aromatic ketones. The strong fluorescent emission was used to track the recovery process of the nanocatalyst very easily [10]. There are only a few reports on the use of heterogeneous chiral Ru(II) amino alcohol complexes as catalysts despite some interesting approaches recently reported [11]. The uses of inorganic amorphous and mesoporous silica support for the preparation of ATH catalysts are still rare. A catalyst non-covalently linked to the silica support introduced by Lemaire [12] showed a good initial performance but suffered from deactivation of the catalyst due to catalyst destruction or leaching of catalytically active metal. A new series of covalently anchored Ru(II) catalysts on the surface of amorphous silica have been reported by Reek and co-workers [13] using (4-chloromethyl)phenyltriethoxysilane as a tethering agent for ATH of acetophenone. It is well known that tethering molecules also greatly affect the activity and enantioselectivity of heterogeneous chiral catalysts. In our previous publication, we have used (4-chloromethyl)phenyltriethoxysilane as a linker molecule to immobilize (1*R*,2*S*)-(+)-*cis*-1-amino-2-indanol on the surface of SBA-15 [14].

Here, we report, the synthesis, characterization, and catalytic applications of heterogeneous Ru(II) complexes of NH-propyl-(1*R*,2*S*)-(+)-*cis*-1-amino-2-indanol for asymmetric transfer hydrogenation of simple ketones. We have also described a detailed characterization that, not only reveals the successful ligand synthesis, functionalization, and immobilization of organic molecules but also displays the structural integrity of the mesoporous support and the Ru(II) complexes inside the material. The performances of the catalysts were studied in the asymmetric transfer hydrogenation of simple prochiral ketones at 60 °C in 2-propanol.

2. EXPERIMENTAL

2.1. Compounds and Materials

Tetraethyl orthosilicate (TEOS), Pluronic P123, (1*R*,2*S*)-(+)-*cis*-1-amino-2-indanol (1*R*,2*S*-AIL), (3-chloropropyl)trimethoxysilane (3-CPTMS), acetophenone (ACP), 4-chloro acetophenone (4-ClACP), 4-bromoacetophenone (4-BrACP), 4-methylacetophenone (4-MeACP), 4-methoxyacetophenone (4-MeOACP), 2,5-dimethoxyacetophenone (2,5-DMeOACP) and propiophenone (PRP) were purchased from Aldrich chemicals (USA). $[\text{RuCl}_2(\text{benzene})]_2$ and $[\text{RuCl}_2(p\text{-cymene})]_2$ were synthesized according to a literature procedure [15]. The reagent grade solvents were obtained from Merck (India) and dried before use according to standard methods. HPLC grade 2-propanol was used for catalytic reactions. The SBA-15 was prepared by hydrothermal crystallization at 100 °C under static conditions for two days using P123 as a structure-directing agent and TEOS as a silica source.

2.2. Synthesis of SBA-15

Siliceous SBA-15 was synthesized by the literature procedure [16] with slight modification. A 4.4 g portion triblock copolymer Pluronic P123 was dissolved under stirring in 30 ml of water for 1.5 h and acidified with (8.724 g/120 ml) of concentrated HCl (pH~1) and stirred again for 2 h at room temperature. Then TEOS (8.526 g, 0.04 mole) was added dropwise with vigorous stirring for 20–30 min and after completion of addition the stirring was continued for 15 min. Thereafter, the homogeneous mixture was maintained at 35 °C for 24 h

without stirring. The resulted heterogeneous mixture was submitted to hydrothermal treatment at 100 °C for 48 h before recovering the solid material. The solid product was filtered, washed with water, and dried in air for 12 h and further in an oven at 70 °C for 5 h. The organic template was removed by calcination in air at 450 °C for 8 h.

2.3. Modification of SBA-15 using 3-CPTMS (Pr-SBA-15)

Calcined SBA-15 (1 g) in dry toluene (30 ml) was refluxed with the required amount of 3-CPTMS for 36 h under an inert atmosphere. The material was filtered after cooling to ambient temperature, washed with dry toluene, and then with dichloromethane. Soxhlet extraction was carried out for 24 h in dichloromethane to remove unattached functional moiety. The sample was dried in a vacuum for 10 h. The dried material was stirred with excess of dimethoxydimethylsilane ($\text{MeO}_2\text{Me}_2\text{Si}$) in dry toluene for 24 h under reflux condition to passivate the undisturbed silanol groups inside and outside the porous material. The filtered sample was washed with dichloromethane several times and dried under vacuum for 10 h. The resultant organo-functionalized material was designated as Pr-SBA-15.

2.4. Ligand Functionalization over Pr-SBA-15 (PrAIL-SBA-15)

Pr-SBA-15 (1 g), triethylamine (0.4 ml), and 1*R*,2*S*-AIL (1.83 mmol, 0.275 g) in 30 ml dry toluene were refluxed for 24 h under inert atmosphere. The resulted material was filtered off, washed initially with dry toluene, and after with an excess of 1:1 dichloromethane and methanol mixture and dried in a vacuum for 10 h. The resulted material was named as PrAIL-SBA-15.

2.5. Complexation of $[\text{Ru}^{\text{II}}\text{Cl}_2(\text{benzene})]_2/[\text{Ru}^{\text{II}}\text{Cl}_2(p\text{-cymene})]_2$ with PrAIL-SBA-15

$[\text{Ru}^{\text{II}}\text{Cl}_2(\text{benzene})]_2/[\text{Ru}^{\text{II}}\text{Cl}_2(p\text{-cymene})]_2$ (30 mg) was taken in dry 2-propanol (40 ml) containing triethylamine (0.15 ml) and refluxed for 1 h under inert condition with stirring after the addition of PrAIL-SBA-15 (1 g). The final brown solid was filtered off and washed with dry 2-propanol for several times, and dried under vacuum for 12 h at 50 °C (Scheme 1). The synthesized materials were named as follows, Ru-1, (catalyst prepared from $[\text{Ru}^{\text{II}}\text{Cl}_2(\text{benzene})]_2$) and Ru-2, (catalyst prepared from $[\text{Ru}^{\text{II}}\text{Cl}_2(p\text{-cymene})]_2$).

2.6. Catalyst Characterization

The structure, phase purity, degree of crystallinity, and unit cell parameters were identified by powder small angle XRD analysis on a SIEMENS D5005 diffractometer using $\text{Cu K}\alpha$ ($\lambda = 0.154$ nm) radiation. The specific surface areas of the samples were determined by the BET method from N_2 adsorption isotherms at 196 °C using an Omnisorb CX-100 Coulter instrument. Before measuring the surface area, the samples were activated at 120 °C for 3 h under a nitrogen atmosphere. The elemental analysis was done with an EA1108 CHN/S Elemental Analyzer (Carlo Erba Instrument) for establishing the presence and exact fraction of elements in the synthesized materials. The metal loading was found with an ICP-AES on a spectroflame D (Spectro analytic instrument). Diffuse reflectance UV-Vis spectra of the powder samples were recorded in the range 200–800 nm on a Shimadzu UV 2101 PC spectrometer equipped with a diffuse reflectance attachment, using BaSO_4 as the reference. A Shimadzu FT-IR 8201 PC Diffuse Reflectance Scanning (DRS) disc technique was used to probe the attached groups and the nature of the surface functional groups in the solid material. 125.757 MHz solid-state ^{29}Si MAS and ^{13}C CP MAS NMR studies were carried out on a Bruker DRX-300 NMR spectrometer. The spectrum was recorded under the Hartmann-Hahn match condition using a contact time of 1 m/sec and a relaxation delay of 4 sec. The size and morphology of the catalyst were measured with

a SEM JEOL-JSM-520 analyzer. The TEM observations were made using a JEOL-JEM-1200 EX instrument with 120kV of acceleration voltage to probe the presence of hexagonal mesophase in the extracted material. XPS measurements were performed on a VG Microtech ESCA 3000 instrument using non-monochromatized Mg K α radiation at pass energy of 50 eV and an electron take-off angle of 60°. The correction of binding energy (B.E.) was performed by using the C1s peak of carbon at 285 eV as a reference. The catalytic activity and enantiomeric excess (*ee*) were measured on an HP 6890 gas chromatograph (GC) equipped with a flame ionization detector and an HP-Chiral 30 m β -cyclodextrin capillary column capillary column (30 m \times 0.32 mm \times 0.25 μ m).

2.7. General Reaction Procedure for Heterogeneous Ru(II) Catalyzed ATH of Ketones in 2-propanol

The heterogeneous catalyst (1 \times 10⁻⁴ mol% Ru content) was taken in a round bottom flask and degassed three times with N₂. Then a stock solution of ketone (0.01 mol%/3 ml 2-propanol) by a syringe followed by KOH solution (0.3 ml, 1 mg/0.1 ml 2-propanol) was added under inert condition. The reaction mixture was stirred at 60 °C for an appropriate time and thereafter the catalyst was separated by centrifugation. The clear solution was washed with ammonium chloride and brine solutions finally with water and separated using diethyl ether. The solution was saturated by high vacuum and the residue was purified by a short silica gel column eluted by ethyl acetate. The catalytic activity and enantiomeric excess (*ee*) were determined by GC analysis.

3. RESULTS AND DISCUSSION

3.1. Powder X-ray Diffraction

The small angle powder XRD patterns [Figure 1] recorded from (a) calcined SBA-15 (b) Pr-SBA-15 (c) PrAIL-SBA-15 (d) Ru-1 (e) Ru-2 samples, in which the strong d₁₀₀ reflection is observed at 2 θ value 0.9° along with the weak d₁₁₀ and d₂₀₀ at 2 θ values 1.51° and 1.75° for all materials. These XRD patterns indicate a high degree of orderedness of the two-dimensional hexagonal (*p6mm*) mesophases of SBA-15 materials prepared at pH \leq 2 [14]. In all the samples, the intensity of the d₁₁₀ reflection is more than the d₂₀₀ reflection. It supports the more complete condensation of the wall structure due to the higher temperatures preferring at hydrothermal synthesis and further calcination. From this, it is confirmed that the calcined SBA-15 material has a stable pore wall thickness to retain its integrity even after several modification treatments. A remarkable decrease in peak intensities to the d₁₀₀, d₁₁₀, and d₂₀₀ reflections was observed for materials after functionalization, ligand immobilization, and further complexation with ruthenium precursors. This indicates the

partial filling of the mesopores by organic moieties due to sequential modification of the SBA-15 material. These results show that the long-range order and structural integrity of the samples were retained after incorporation of organometallic complexes [14].

3.2. N₂-sorption Studies

The specific surface area, pore volume, and pore diameter were estimated from N₂ sorption isotherms [Figure 2] and pore size distribution [Figure 3] of the (a) SBA-15, (b) Pr-SBA-15, (c) PrAIL-SBA-15, (d) Ru-1 and (e) Ru-2 and the values were displayed in Table 1. All the materials exhibited type IV isotherm (definition by IUPAC) with H₁-type hysteresis that is typical of mesoporous materials with cylindrical channels possessing pore diameters between 2 and 50 nm [14]. The surface area, pore diameter and pore volume values of SBA-15, Pr-SBA-15, PrAIL-SBA-15, Ru-1 and Ru-2 were found to be 854 m²g⁻¹, 78 Å, 1.16 cm³g⁻¹; 598 m²g⁻¹, 72 Å, 0.80 cm³g⁻¹; 477 m²g⁻¹, 66 Å, 0.69 cm³g⁻¹; 419 m²g⁻¹, 64 Å, 0.58 cm³g⁻¹ and 412 m²g⁻¹, 64 Å, 0.59 cm³g⁻¹, respectively. The samples showed a remarkable decrease in surface area on progressing the surface modification process and the ligand-modified samples obviously exhibit lower specific surfaces than the parent solids due to the introduction of the organic moieties (ligands and/or Me₂-Si groups), which is also responsible for a reduction of

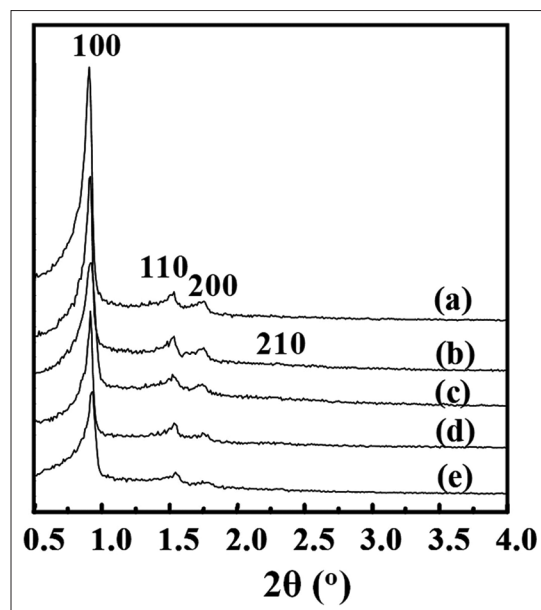


Figure 1: Low angle XRD patterns of (a) SBA-15, (b) Pr-SBA-15, (c) PrAIL-SBA-15, (d) Ru-1 and (e) Ru-2

Table 1: Physico-chemical properties of synthesized materials.

Material	% of Ru ^a (w/w)	BET adsorption-desorption Measurements ^b			Core level energies (in eV) of various elements ^c				
		Surface area (m ² g ⁻¹)	Pore diameter (Å)	Pore volume (cm ³ g ⁻¹)	Ru 3d5/2	Ru 3p3/2	N 1s	Si 2p	O 1s
SBA-15	----	854	78	1.16	----	----	----	----	----
Pr-SBA-15	----	598	72	0.80	----	----	----	----	----
PrAIL-SBA-15	----	477	66	0.69	----	----	----	----	----
Ru-1	0.51	419	64	0.58	280.2	464	401.8	103.5	533.0
Ru-2	0.52	412	64	0.59	280.2	464	401.8	103.5	533.0

^aAnalyzed by ICP-AES to measure the total metal complex loading (Wt/g in 100 g of heterogeneous catalyst).

^bMeasured by N₂ adsorption-desorption at -196°C.

^cThe core level binding energies were aligned with respect to the C 1s binding energy of 285 eV using adventitious carbon.

pore volumes and pore diameters. A specific surface area decrease of Pr-SBA-15 and PrAIL-SBA-15 were about 30 and 44%, respectively, after the functionalization of calcined SBA-15, which points out the anchoring of a considerable amount of organic molecules inside the pores of calcined silica support. Further a small decrease in the specific surface area of Ru-1 and Ru-2 *ca.* 419 and 412 m^2g^{-1} , respectively, evidenced the successful complexation of the immobilized ligand by ruthenium precursors. The surface area values were found to be nearly similar for Ru-1 and Ru-2 indicates an agreement in metal loading in both the heterogeneous catalysts.

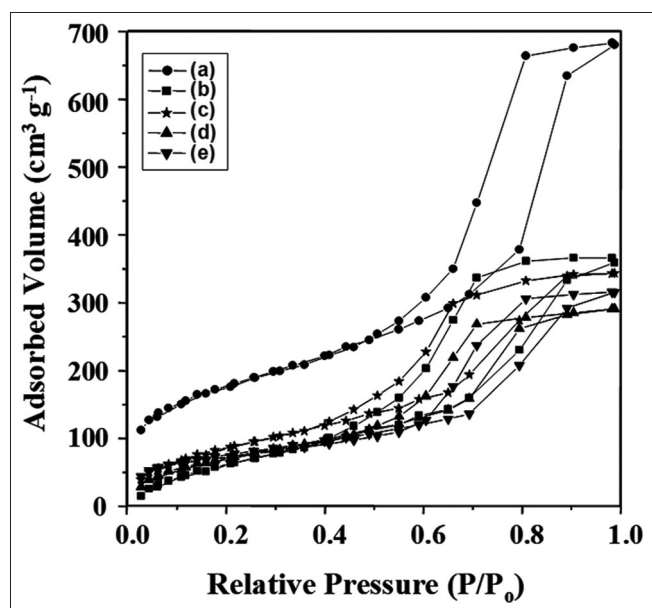


Figure 2: N₂-sorption isotherms of (a) SBA-15, (b) Pr-SBA-15, (c) PrAIL-SBA-15, (d) Ru-1 and (e) Ru-2

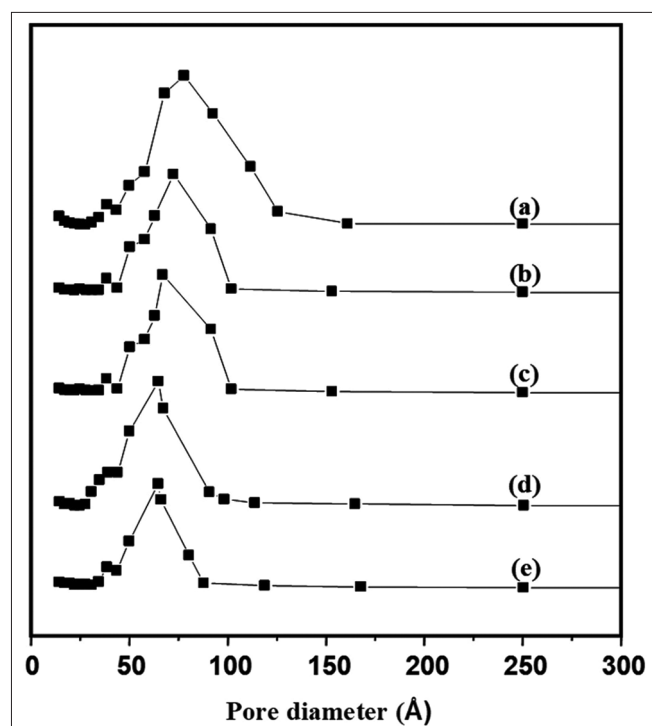


Figure 3: Pore size distributions of (a) SBA-15, (b) Pr-SBA-15, (c) PrAIL-SBA-15, (d) Ru-1 and (e) Ru-2

A broad pore size distribution with a mean value of 78 Å is found for both the adsorption and desorption processes for calcined SBA-15. However for the modified materials (Pr-SBA-15, PrAIL-SBA-15, Ru-1, and Ru-2), partially narrow and lower pore size distributions were obtained (72–64 Å), which might imply that the chelating ligand and the Me_2Si - groups are moreover uniformly distributed all over the SBA-15 channel surface in these samples [17]. The insertion of organic molecules inside the channels of the mesoporous materials has been further evidenced from the measurement of the pore volume of the synthesized materials. The pore volume is considerably decreasing after functionalization, immobilization of ligand, and further metal complex addition to the calcined SBA-15, indicates the progress of anchoring of the organic moieties inside the channels. However, only a small amount of decrease in pore volume from the PrAIL-SBA-15 has observed after the addition of metal precursors, which is further supported by the pore diameter values of these materials that also did not change considerably while complexation.

3.3. Microscopic Studies

It is now apparent that morphology and texture of mesoporous silica are extremely important and it may vary with synthesis parameters [14,17,18]. Figure 4 shows the TEM images of calcined SBA-15, (a) along the pore direction and (b) perpendicular to the channels. The images revealed the formation of a regular hexagonal array of uniform channels having long-range order and the image exposed the formation of well-defined one-dimensional channels. These results further support the XRD results described previously. Figure 5 represents the SEM images of (a) SBA-15, (b) Pr-SBA-15, (c) PrAIL-SBA-15, (d) Ru-1, and (e) Ru-2. Calcined SBA-15 shows aggregated polygonal disc-like morphology having a particle size of *ca.* 2 μm and it reveals a well-distributed hexagonal material, which is earlier predicted from XRD patterns [14,16,17]. The particle size is intact even after progressive modifications but a slight change in morphology was observed from polygonal disc to normal disk structure, which is due to the prolonged contact of the material with solvents at various synthesis conditions.

3.4. FT-IR Study

The proper functionalization of the organic moieties is confirmed from the FT-IR spectroscopic analysis of (a) Pr-SBA-15 (b) PrAIL-SBA-15 (c) Ru-1 and (d) Ru-2 and presented in Figure 6A and B. In the entire spectrum, a broadband was observed between 3800 and 3000 cm^{-1} , which corresponds to the O-H stretching vibrations. The broadness might be due to the hydrogen bonding with each other. In addition, in calcined SBA-15 a sharp band between 1650 and 1600 cm^{-1} is due to the bending vibrations of surface O-H groups and water molecules occluded in the pores. In all the samples a sharp peak at 800 cm^{-1} is observed, which is due to the Si-O stretching bond. In the entire spectrum, two weak bands at around 3000–2900 cm^{-1} corresponding to asymmetrical and symmetrical stretching vibrations of $-\text{CH}_2$ groups of the organic moieties [17,19]. In addition to these bands a broad

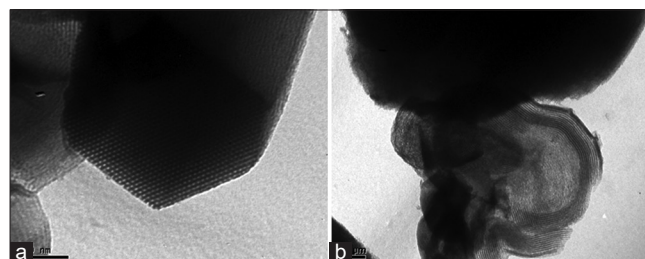


Figure 4: was aligned (a) parallel to the main axis of the channel, and (b) perpendicular to the main axis of the channel

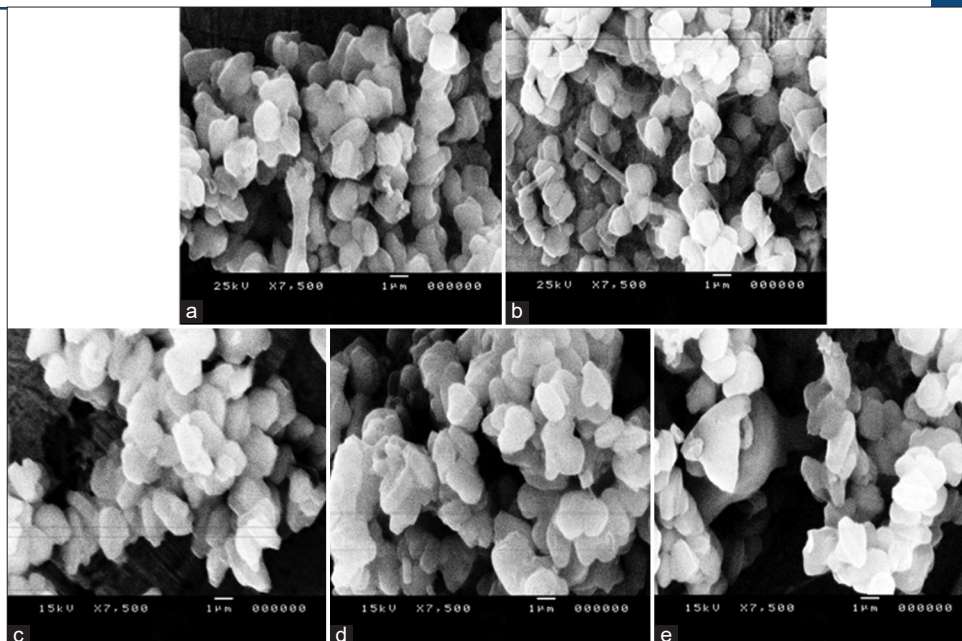


Figure 5: Scanning electron micrographs (SEM) of (a) SBA-15, (b) Pr-SBA-15, (c) PrAIL-SBA-15, (d) Ru-1 and (e) Ru-2

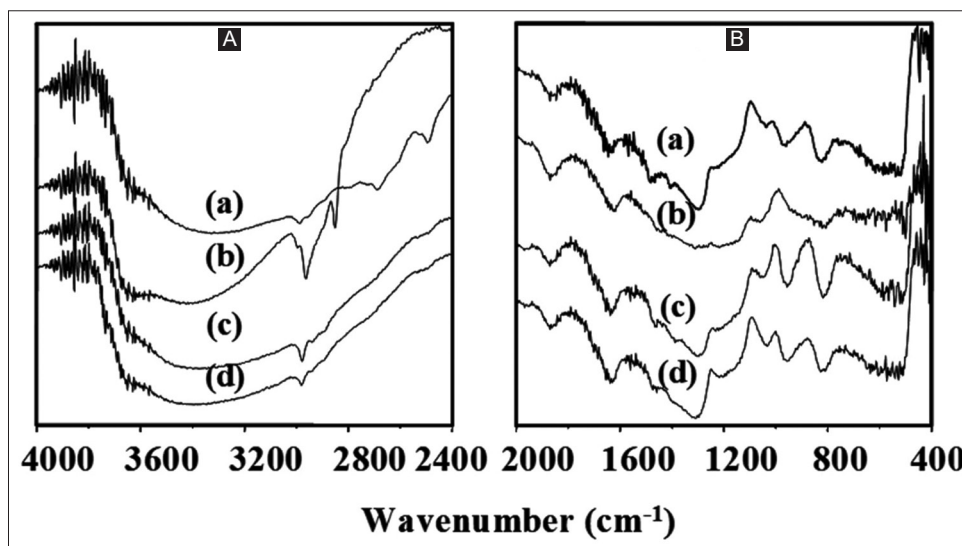


Figure 6: A and B are the FT-IR spectra of (a) Pr-SBA-15, (b) PrAIL-SBA-15, (c) Ru-1 and (d) Ru-2

peak at around $1400\text{--}1250\text{ cm}^{-1}$ is due to the C-H bending vibration of the functionalized moieties. A medium sharp band at around $1650\text{--}1600\text{ cm}^{-1}$ is indexed to the surface silanol groups, which is further confirmed from the broadband at around $3800\text{--}3000\text{ cm}^{-1}$. In addition to the above band, the entire spectra show two weak bands at around $3200\text{--}2800$ and $1500\text{--}1300\text{ cm}^{-1}$ which are due to the C-H stretching and bending vibrations of methylene group of functionalized and ligand molecules. In the ligand immobilized material, we have expected a weak band at 3260 cm^{-1} for the -NH stretching vibration, which is unresolved due to the overlapping of O-H stretching vibration (3400 and 3650 cm^{-1}) of surface O-H groups and water molecules occluded in the pores [19]. A small and broadband in all spectrums at 702 cm^{-1} represents the C-H bending vibration of the methylene group of benzene. It is also observed that a medium band at 1423 cm^{-1} indicates the C=C stretching in-plane vibration of the benzene framework. A band at 707 cm^{-1} represents the C-H bending vibration of benzene.

3.5. Solid-state NMR Spectra

The ^{13}C CP MAS and ^{29}Si MAS NMR spectra of the synthesized materials not only disclosed the structural information of the synthesized support material but also removed the ambiguity on the successful functionalization and further immobilization of the ligand over SBA-15. From ^{13}C CP MAS NMR spectra [Figure 7], one could see the signals at chemical shifts characteristics of the organic moieties attached on the surface of (a) PrCl-SBA-15, (b) Pr-SBA-15 and (c) PrAIL-SBA-15. In the spectrum of PrCl-SBA-15, three sharp peaks at chemical shift values 9 ppm, 26 ppm, and 46 ppm were observed. These signals were assigned to the carbons 1, 2, and 3, respectively, in PrCl-SBA-15 [Figure 7a] [17,20]. In Pr-SBA-15 an additional resonance was observed at $\delta = -3$ ppm along with the three resonances of the propyl carbons, which was attributed to the -CH₃ carbon (numbered as 4) of the protecting molecule [Figure 7b]. The simultaneous presence of peaks of carbons in chloropropyl group and methyl group suggest that these two groups were grafted on

mesoporous SBA-15. For PrAIL-SBA-15, the ^{13}C CP MAS NMR spectrum shows the persistence of the tethering molecule and the protecting group and few signals at chemical shift values 40, 64, 74, 126, and 141 ppm due to the anchored ligand molecule. In the ligand molecule three types of sp^3 hybridized carbons (numbered as 5, 6, and 7, Figure 7c) and two classes of sp^2 hybridized carbon centers were present (numbered as 8 and 9, Figure 7c). The resonances at 40, 64 and 74 ppm were corresponding to the carbon atoms 5, 6 and 7. The peaks at chemical shift values 126 and 141 ppm were responsible for the phenyl ring [17,20] in the ligand molecule (numbered as 8 and 9, Figure 7c). The above results evidenced the successful anchoring of tethering, protecting, and ligand molecules on mesoporous SBA-15.

Figure 8 represents the ^{29}Si MAS NMR spectra of (a) calcined SBA-15, (b) PrCl-SBA-15, and (c) Pr-SBA-15. In the entire spectrum, the strong resonances at $\delta \approx -112$, -102 and -93 ppm are attributed to Q^4 [$\text{SiO}_3=\text{Si}-\text{O}-\text{Si}=\text{}$], Q^3 [$(\text{SiO}_3=\text{Si}-\text{OH})$] and Q^2 [$(\text{SiO}_2=(\text{Si}-\text{OH})_2)$] species, respectively, present in the silicate framework of SBA-15, PrCl-SBA-15, and Pr-SBA-15 [19]. The Q^3 sites are associated with isolated Si-OH groups, and the Q^2 sites correspond to geminal

silanediols. For the modified sample [Figure 8b] three additional broad and overlapping signals appear at -78 , -70 , and -60 ppm, which can be assigned to T^3 , T^2 , and T^1 organosilica species [17,20], respectively, with T^2 as the major system. Parallely, the relative intensity of the Q^2 resonances decreases with a slight increase of Q^4 . For Figure 8c, grafting of the dimethylsilane groups to SBA-15 further decreases the intensity of the Q^2 resonances (almost to the detection limit) and drastically increases the intensity of the Q^4 silicon atoms, while a broad peak at -15 ppm with a shoulder peak at -8 ppm can be assigned to the silicon nuclei of the dimethylsilyl ($\text{Me}_2\text{Si}-$) groups [21]. Changes in the relative intensities of the Q^4 , Q^3 , and Q^2 signals can be explained by the redistribution of the silicon sites during surface silylation. The relative intensity of the Q^4 site is very high when comparing with the Q^3 site indicates the formation of a highly condensed stable silica framework. The presence of Q^3 sites indicates the availability of enough surface silanol groups for functionalization. The results presented above suggest that the activity and recyclability of the modified mesoporous material can be improved by a decrease of the number of surface Si-OH groups using $\text{Me}_2\text{MeO}_2\text{Si}$ as the silylating agent. As only a small part of the Si-OH groups are consumed during the introduction of the ligand system, the remaining Si-OH groups will provide centers for the adsorption of organic compounds by hydrogen bonding, which will hinder the diffusion to and away from the catalytically active centers in the mesoporous cavities and therefore decrease the overall activity of the catalyst. Our NMR spectroscopic investigations prove that by reacting the surface with $\text{Me}_2\text{MeO}_2\text{Si}$ converts a major part of the Si-OH groups into Si-O-SiMe₂ groups and therefore increases the hydrophobicity, which will reduce adsorption effects [16,17].

3.6. UV-Vis Studies

Figure 9 illustrates the UV-Vis spectra of Ru-1 (a) and Ru-2 (b). Sharp peaks at 422 and 424 nm have been observed for Ru-1 and Ru-2, respectively, metal-to-ligand charge-transfer (MLCT) bands, indicates the anchoring of the complex on the surface-modified SBA-15 [17,22]. The small difference in absorption peaks might be due to the presence of different aromatic rings (benzene and *p*-cymene for Ru-1 and Ru-2, respectively) in the complex materials.

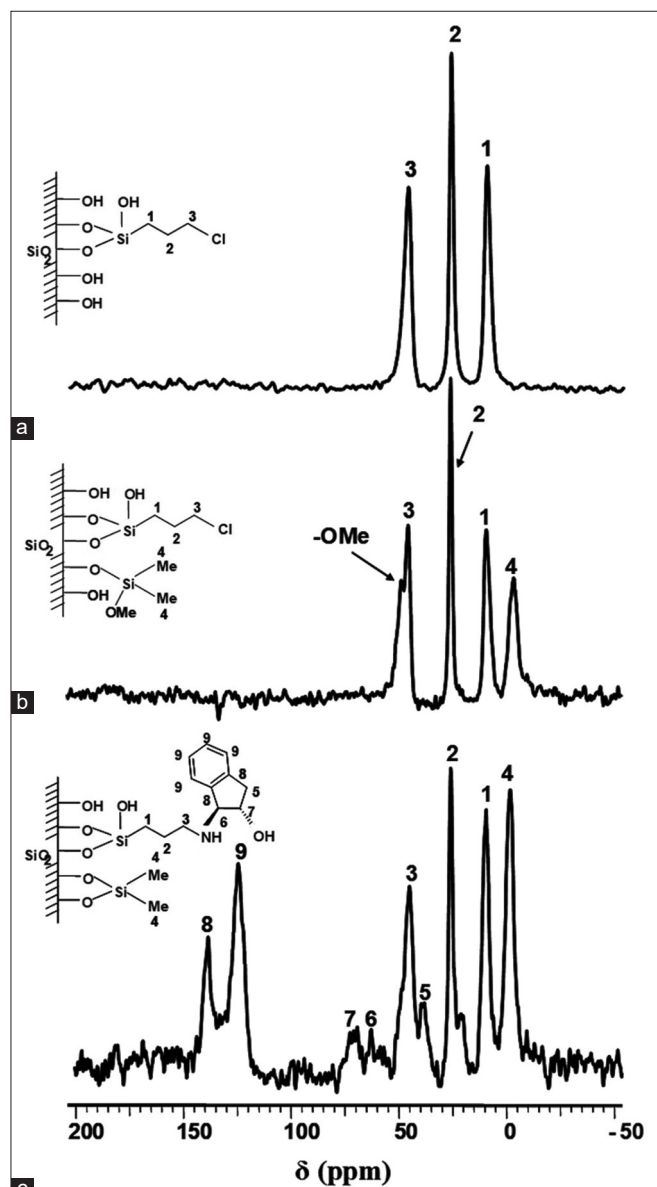


Figure 7: ^{13}C CP-MAS NMR spectra of (a) PrCl-SBA-15 (b) Pr-SBA-15 and (c) PrAIL-SBA-15

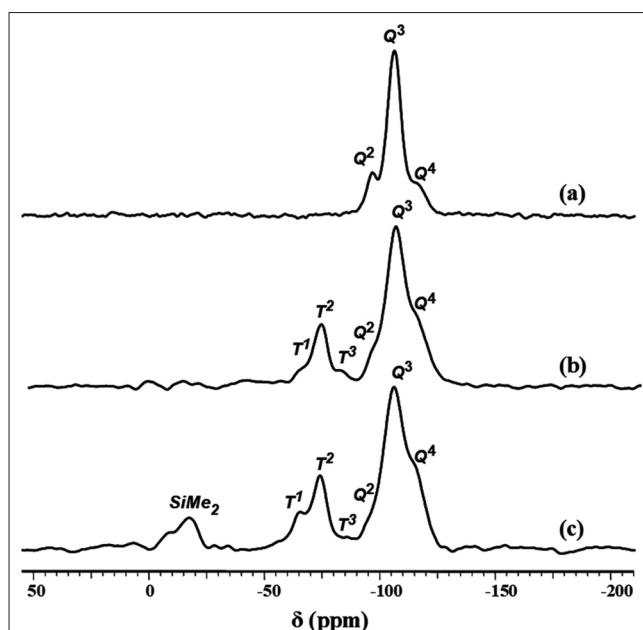


Figure 8: ^{29}Si MAS NMR spectra of (a) SBA-15, (b) PrCl-SBA-15 and (c) Pr-SBA-15

3.7. X-ray Photoelectron Spectra (XPS)

Usually, the binding energy (BE) of an electron depends strongly not only upon the level from which photoemission occurs but also upon the formal oxidation state of the atoms and the local chemical and physical environments of the resulting compounds [23]. Surface analytical information of the synthesized samples was obtained by XPS analysis and has given additional support for the successful anchoring of the Ru(II) complexes onto the solid support [Figure 10]. Table 1 also demonstrates the Ru3d_{5/2}, Ru3p_{3/2}, N1s, Si2p, and O1s core level

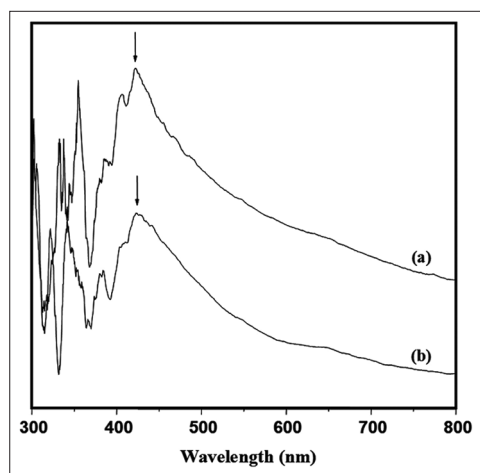


Figure 9: UV-Vis spectra of (a) Ru-1 and Ru-2

binding energies (BE) obtained from XPS analysis of the synthesized materials. All the samples exhibit two BE values of 103.5 and 533.0 eV correspond to the Si2p and O1s core level of the silica material, which is matching with the literature values very well [22]. The BE value of 401.8 eV corresponding to N1s core level of the 1R,2S-AIL ligand. We have used the BE values from XP spectra in the range from 279 to 297.5 eV to clarify the oxidation state of the ruthenium. The peaks that are visible in this region are due to the presence of Ru (3d_{5/2} and 3d_{3/2}) and carbon (C 1s) electron transitions. After complexing with [RuCl₂(benzene)]₂ and [RuCl₂(*p*-cymene)]₂, we have noticed two additional BE values at *ca.* 280–283 and 464 eV correspond to core level BE's of Ru 3d_{5/2} and Ru 3p_{3/2}, respectively. For both the catalysts (Ru-1 and Ru-2), we could have observed a small peak at 280.2 eV for Ru 3d_{3/2}, which partially overlapping with the C 1s (285 eV) peak but the Ru 3p_{3/2} peak has observed at 464 eV. These binding energies correspond to a Ru(II) species and it proved not only the structural integrity of the ruthenium precursors but also the unchanged oxidation state of the metal ion even after anchoring with the ligand molecule. The peaks were energy-shifted to the binding energy of C 1s (285 eV) to correct the charging of the material [24].

3.8. ATH of Simple Prochiral Ketones

All heterogeneous catalysts prepared in this study were exploited in the enantioselective transfer hydrogenation of simple aromatic ketones and the results are summarized in Table 2. From the table, it is evidenced that a greater part of all the substrates were reduced with moderate to high enantiomeric excess within a short period of time.

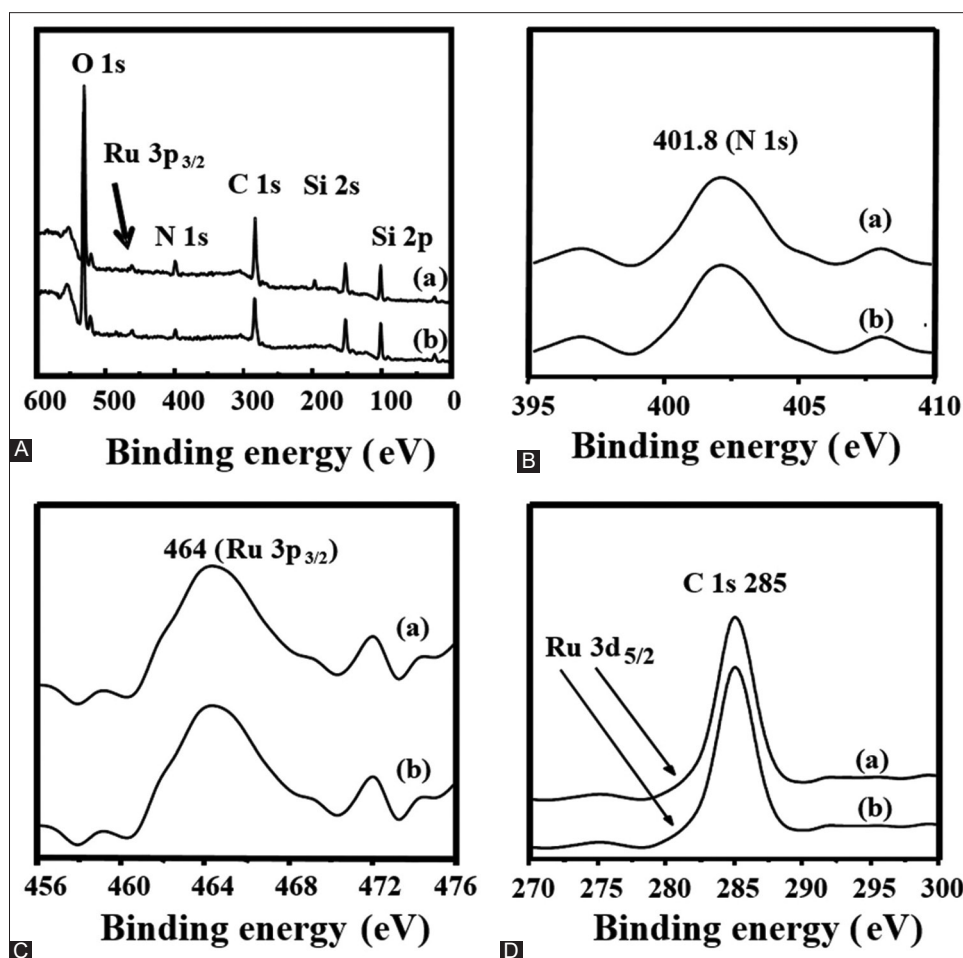


Figure 10: XPS spectra of (a) Ru-1 and (b) Ru-2. (A) Full range spectra (B) N1s binding energy of ligand (C) binding energies of Ru3p_{3/2} electrons and (D) binding energies of C1s and Ru3d_{5/2} electrons

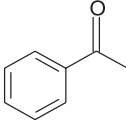
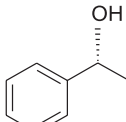
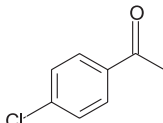
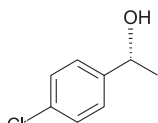
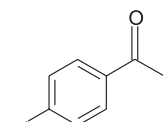
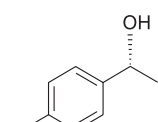
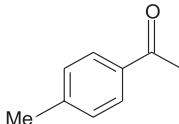
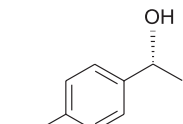
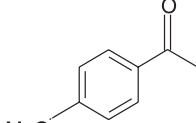
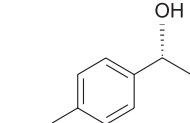
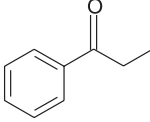
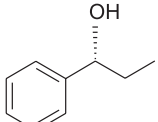
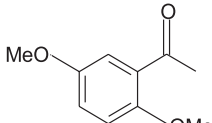
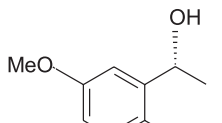
Here we report an overall kinetic expression using acetophenone as a model compound and exploited the excellent performance of Ru-1 in 2-propanol. The influences of reaction time, temperature, amount of solvent, and amount of base have been investigated. To get an insight about the stability and activity of recycled catalysts, we have conducted the recycling study of Ru-1 and Ru-2 for a maximum of three recycling runs in the ATH of acetophenone under similar reaction conditions and the results were summarized in Table 3.

3.8.1. Different Substrates

Phenyl alkyl ketones (PhCOAlkyl) are the substrates of choice for the assessment of the synthesized catalysts in the transfer hydrogenation reaction (Scheme 2). For a given catalytic system, rate, and selectivity are sensitive to the steric crowding of the substrates as well as to the electronic properties of the phenyl ring substituents. Later it is proved

that along with the substrates the electronic and structural constrains of the active center of the catalyst itself can control the activity and enantioselectivity [25,26]. The presence of an electron-withdrawing group on the phenyl ring has generally been found to facilitate the hydrogen transfer reaction and this has been attributed to the hydridic nature of the reducing species involved. As such, due to the fast hydride transfer, the reactions of -Cl, -Br, or -OCH₃ substituted substrates should proceed at a higher rate, while reactions with electron-donating substituents (-CH₃) should proceed with a more controlled manner. To elucidate the catalytic activity and enantioselectivity of the synthesized catalysts, the reaction has performed a procedure similar to the methodology available in literature for chiral amino alcohol complexes [9]. Results are presented in Table 2. All the reactions were carried out under similar conditions in a batch reactor using 2-propanol

Table 2: Asymmetric transfer hydrogenation of simple prochiral ketones.^a

Entry	Substrate	Product	Ru-1		Ru-2	
			Conversion (%) ^b	ee (%) ^b	Conversion (%) ^b	ee (%) ^b
1			62	66*	40	88*
2			83	48	40	85
3			88	48	53	84
4			43	60	28	86
5			58	60	32	86
6			77	64	41	84
7			56	52	26	86

^aThe reaction was carried out at 60°C for 1 h, using 0.01 mol % of ketone and a S/C ratio of 100 in 3 mL solvent. KOH=3 mg/0.3 mL 2-propanol.

^bDetermined by GC equipped with a chiral column. The configuration of alcohol product was S.

*Configuration was found by comparing with authentic compound. All other configurations were found by comparing R_f values with R_f values published in literatures.

as solvent as well as a proton source. The use of 0.01 mol% prochiral ketones in conjunction with 1×10^{-4} mol% of the ruthenium complex (Ru-1/Ru-2) and 3 mg of KOH in 2-propanol (0.3 ml) at 60 °C temperature resulted in the enantioselective reduction of prochiral ketones to corresponding (*S*)-alcohol [17,27,28].

Acetophenone reduced 62 and 40% with *ee* values of 66 and 88% for Ru-1 and Ru-2, respectively, (entry 1) within 1 h. For instance, 4-chloroacetophenone and 4-bromoacetophenone were reduced to

Table 3: Recyclability of the catalysts in the asymmetric transfer hydrogenation of acetophenone.^a

Entry	Cycle	Ru-1		Ru-2	
		Conv. (%) ^b	<i>ee</i> (%) ^b	Conv. (%) ^b	<i>ee</i> (%) ^b
1	Fresh	62	66	40	88
2	First	56	66	22	88
3	Second	31	66	12	88
4	Third	10	66	5	88

^aThe reaction was carried out at 60°C for 1 h, using 0.01 mol% of ketone and

S/C ratio of 100 in 3 ml solvent. KOH = 0.3 ml (1 mg/0.1 ml 2-propanol).

^bDetermined by GC equipped with a chiral column.

83 and 88%, and the highest conversion among the substrates (For Ru-1) having *ee* values of each 48% (entry 2 and 3) were obtained. However for the Ru-2 catalyst, lower activities (40 and 53%) with enhanced *ee* values (85 and 84%) have been observed (entry 2 and 3). The reduction of 4-methylacetophenone gave 43% conversion with 60% *ee* for Ru-1 and 28% conversion with 86% *ee* for Ru-2 (entry 4). 4-methoxyacetophenone reduced to 58% conversion with 60% *ee* for Ru-1 and 32% conversion with 86% *ee* for Ru-2 (entry 5). It is believed that a *p*-methoxy group in acetophenone significantly decreases the enantioselectivity. 2,5-dimethoxyacetophenone exhibited a moderated conversion (77%) and less *ee* (64%) for Ru-1 and 41% conversion and 84% *ee* for Ru-2 (entry 6). Propiophenone exhibited a yield of 77% and *ee* of 64% for Ru-1 and 41% yield and 84% *ee* for Ru-2 (entry 6). 2,5-dimethoxyacetophenone (entry 7) exhibited is comparably lower conversion and *ee* for both Ru-1 (56 and 52%) and Ru-2 (26 and 86%) than 4-methoxyacetophenone due to steric hindrance exerted by the methoxy groups in the ortho and meta positions to the carbonyl group that may cause the access of the carbonyl carbon to the Ru(II)-H hydride. From the results, it is observed that the heterogeneous catalyst Ru-1 displayed higher conversion than the catalyst Ru-2 for simple prochiral ketones. However, the *ee* results are superior for Ru-2 than Ru-1 at our reaction conditions and may be due to the favorable special arrangement of sterically hindered *p*-cymene in the metal complex. As a general strategy, the results with the substituted acetophenones suggested that electron-withdrawing groups show higher substrate

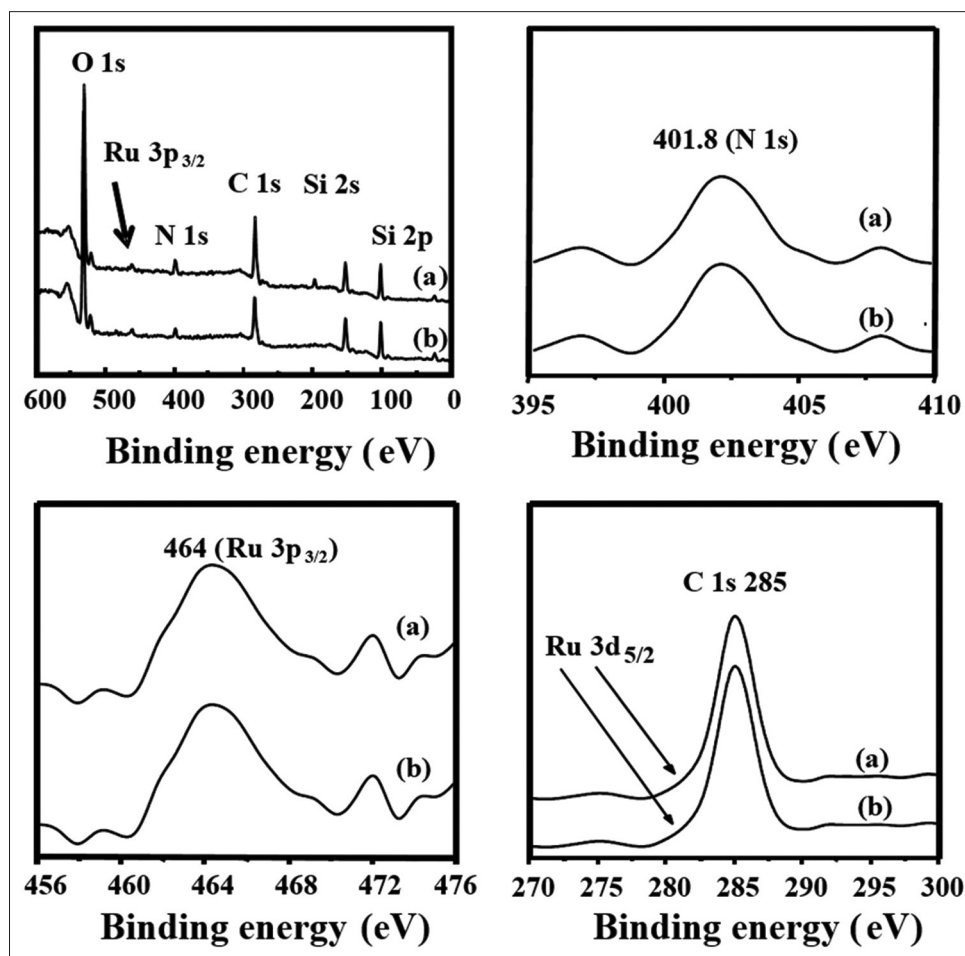
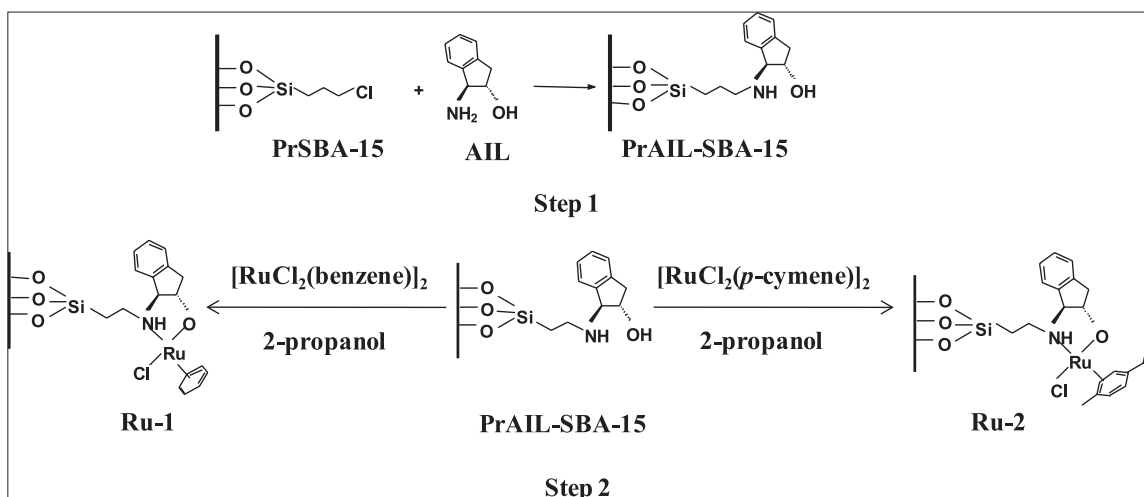
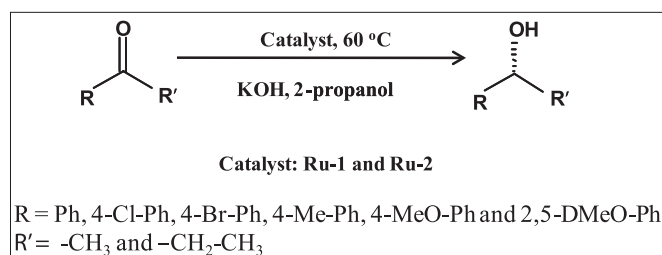


Figure 11: Influence of reaction temperature (a), time (b), amount of solvent (c) and amount of base (d) on conversion and enantioselectivity in the asymmetric transfer hydrogenation of acetophenone by Ru-1. Reaction conditions: For (b), (c) and (d) temperature = 60 °C. For (a), (c) and (d) time = 1 h. For (a), (b) and (d) amount of solvent (2-propanol) = 3 ml. For (a), (b) and (c) amount of base = 0.3 ml, Acetophenone = 0.01 mol%, S/C ratio = 100, KOH = 1 mg/0.1 ml 2-propanol.



Scheme 1: Synthetic approach to heterogenize Ru(II)-NH-propyl-(1R,2S)-(+)-cis-1-amino-2-indanol complexes on SBA-15. Step 1. Preparation of immobilized NH-propyl-(1R,2S)-(+)-cis-1-amino-2-indanol and Step 2. Preparation of Ru-1 and Ru-2



Scheme 2: Asymmetric transfer hydrogenation of simple prochiral ketones in 2-propanol

conversions than electron-donating groups. The enantiomeric excess results are exactly the reverse to the conversion strategy. Electron-withdrawing substituents in para-substituted acetophenones instead tend to slightly decrease the enantioselectivities [17,19].

3.8.2. Influence of reaction time over conversion and enantioselectivity

The influence of reaction time over the conversion and enantioselectivity in the transfer hydrogenation of acetophenone is presented in Figure 11a. We have conducted the experiment for 15 min (31% conv. and 66% *ee*), 30 min (41% conv. and 66% *ee*), 1 h (62% conv. and 66% *ee*), 2 h (78% conv. and 66% *ee*), 5 h (85% conv. and 63% *ee*) and 10 h (86% conv. and 60% *ee*). The results illustrate that the conversion increases with time, as expected, and reaches an optimum value (86%) before 10 h in the case of the Ru-1. The *ee* values, however, attain a maximum (66%) from the very beginning of the reaction. However for 5 and 10 h the *ee* values decreased to 63 and 60%, respectively [29-32].

3.8.3. Influence of reaction temperature over conversion and enantioselectivity

Figure 11b demonstrates the performance (conversion and enantioselectivity) of Ru-1 under various reaction temperatures in the transfer hydrogenation of acetophenone and the results are mentioned in brackets. We have selected 0 °C (3% conv. and 70% *ee*), 40 °C (49% conv. and 70% *ee*), 60 °C (62% conv. and 66% *ee*) and 80 °C (68% conv. and 64% *ee*) for our study. The results demonstrate that the ATH of acetophenone is temperature-dependent. As the temperature increases the activity of the catalyst also increases. However, the *ee* value decreased from 70 to 64% as expected. It proved that at lower temperatures (0 and 40 °C) the reaction prefers the production of *S* isomer and at higher temperatures (60 and 80 °C) a marginal production of *R* isomer is taking place. It is also noticed that the activity of the

catalyst is not remarkable when going from 60 (conv. 62%) to 80 °C (conv. 68%).

3.8.4. Influence of amount of solvent over conversion and enantioselectivity

The effect of the amount of solvent (2-propanol) over the conversion and enantioselectivity in the ATH of acetophenone is presented in Figure 11c. It is accounted that 2-propanol is acting as a solvent and the proton donor simultaneously. During the course of the reaction, it releases a proton and converts itself to acetone. Due to the reversibility nature of the process, here is a chance to accept a proton from the reaction products (*S* and *R*-1-phenylethanol) to change back to 2-propanol. Hence, it is necessary to keep an optimum dilution in the reaction system to prevent the backward reaction. We have studied the asymmetric reduction of acetophenone keeping 1 ml (63% conv. and 66% *ee*), 3 ml (62% conv. and 66% *ee*), 5 ml (47% conv. and 68% *ee*) and 10 ml (34% conv. and 72% *ee*) solvent in the reaction system. The results illustrate that while increasing the solvent amount from 1 ml to 10 ml the activity goes on decreasing from 63 to 34%. However, the *ee* value increased considerably from 66 to 72% while increasing the amount of solvent. Hence, for the reaction, 1 ml or 3 ml of solvent is suitable for obtaining a maximum conversion. We have selected a 3 ml solvent for the ATH of various substrates for considering other factors such as base concentration and reaction temperature.

3.8.5. Influence of amount of base over conversion and enantioselectivity

It is well-known and experimentally proved that the transfer hydrogenation of prochiral ketones is no more initiating in the absence of a base. Hence, it is obvious that the presence and the amount of base have a strong influence in the reaction rate. We have used 0.1 ml (59% conv. and 66% *ee*), 0.2 ml (60% conv. and 66% *ee*), 0.3 ml (62% conv. and 66% *ee*) and 0.4 ml (82% conv. and 64% *ee*) base solution from a 0.18 M solution of KOH in 2-propanol for our study and is shown in Figure 11d. It was manifested that while increasing the amount of base the reaction rate increased slightly (from 59 to 62%) and the enantioselectivity (66%) was intact up to 0.3 ml of the base solution. However, the reaction rate is drastically increased to (82%) and the enantioselectivity goes down to (64%) along which, the reaction mixture turned colored when using 0.4 ml of the base solution. The ICP-AES analysis proved the presence of leached metal complexes in the reaction residue after centrifuged out the catalyst. Hence, we have confirmed that the noticed higher activity is due to the leached active metal complexes when using 0.4 ml base solution. The decreased

enantioselectivity is due to the progressive reaction rate by the leached metal complex in the solution.

3.8.6. Recycling study

The recycling study was effectively worked out by centrifuging the reaction mixture for 3–5 min after 1 h of the reaction and the solution was removed with a syringe. The catalyst was washed with dry 2-propanol (1 ml, thrice) and the solutions were removed with a syringe. A new reaction could be conducted by adding a stock solution of ketone (0.01 mol%/3 ml 2-propanol) by a syringe followed by KOH solution (0.3 ml, 1 mg/0.1 ml 2-propanol) under inert conditions. As seen in Table 3, the fresh heterogeneous catalysts Ru-1 and Ru-2 exhibited good catalytic activity and enantioselectivity for acetophenone under our reaction conditions. In the consecutive runs, the catalysts showed a decrease in catalytic activity without losing the enantioselectivity [8,17].

4. CONCLUSION

Highly reactive heterogeneous catalytic systems were developed by immobilizing 1R,2S-AIL over SBA-15, and further complexation was carried out with $[\text{RuCl}_2(\text{benzene})]_2$ and $[\text{RuCl}_2(p\text{-cymene})]_2$. The powder XRD patterns confirmed the formation of the siliceous SBA-15 material and the integrity of its mesoporous nature throughout the modification process. The N_2 adsorption-desorption studies ascribed the high surface area and considerable pore size distribution, which is in general agreement with previous reports on mesoporous SBA-15. The TEM images were strongly supported the XRD and N_2 adsorption-desorption results. ^{13}C CP MAS NMR studies disclosed the unambiguity in the anchoring of 3-CPTMS and 1R,2S-AIL over SBA-15. FT-IR showed the major vibrational frequencies of functional groups present in the anchored ligand and the metal complexes, which further supported the NMR results. The loading of ruthenium complexes over ligand immobilized SBA-15 has been confirmed by UV-Vis analysis and further, the amount of active metal was determined by the ICP-AES analysis of Ru-1 and Ru-2. The XPS study was revealed the presence and the proper complexation of ruthenium species with the chelating immobilized chiral ligand. These mesoporous SBA-15-supported chiral catalysts were used for the enantioselective transfer hydrogenation of a range of simple prochiral ketones with good to excellent conversions and enantioselectivity under mild reaction conditions. It is noticed that the substrate having electron-withdrawing groups in the para position of the aromatic ring showed higher conversion but a decreased enantiomeric excess it is exactly opposite to the substrates having electron-donating groups in their para position. From the comparative reactivity studies of Ru-1 and Ru-2, it was noticed that Ru-1 is catalytically more active and enantiomerically less selective than Ru-2. Acetophenone has given a maximum of 62% conversion and 66% *ee* for Ru-1 and 40% conversion and 88% *ee* for Ru-2. The recyclability of the catalysts was effective up to the second recycling step after that an immediate deactivation was observed. It was observed that the heterogeneous catalyst prepared from $[\text{RuCl}_2(\text{benzene})]_2$ displayed higher conversion than the catalyst prepared from $[\text{RuCl}_2(p\text{-cymene})]_2$ for the enantioselective reduction of simple prochiral ketones. However, the enantiomeric excess results are vice versa and may be due to the favorable special arrangement of sterically hindered *p*-cymene toward enantioselection in the metal complex. While monitoring the reduction of acetophenone over Ru-1 it was noticed that the reaction rate was fast initially while later the rate decreased as the reaction proceeds. The kinetic study using heterogeneous modified Ru(II)-(1R,2S)-(+)-*cis*-1-amino-2-indanol reveals that the reaction conditions such as temperature, duration of reaction, amount of base, and amount of solvent have a strong influence over both conversion and enantiomeric excess. The catalysts recycled to a maximum of three successive runs. All the heterogeneous catalysts

show a drastic decrease in activity from the first recycling experiment onward without changing the enantiomeric excess considerably.

5. ACKNOWLEDGMENT

S. P. thanks to the National Chemical Laboratory (NCL), Pune, Maharashtra for characterizing the materials.

REFERENCES

1. J. Wu, J. X. Ji, R. Guo, C. H. Yeung, A. S. C. Chan, (2003) Chiral $[\text{RuCl}_2(\text{dipyridylphosphane})(1,2\text{-diamine})]$ catalysts: Applications in asymmetric hydrogenation of a wide range of simple ketones, *Chemistry: A European Journal*, **9**: 2963-2968.
2. F. Foubelo, C. Nájera, M. Yus, (2015) Catalytic asymmetric transfer hydrogenation of ketones: Recent advances, *Tetrahedron Asymmetry*, **26**: 769-790.
3. S. Hashiguchi, A. Fuji, J. Takehara, T. Ikariya, R. Noyori, (1995) Asymmetric transfer hydrogenation of aromatic ketones catalyzed by chiral ruthenium(II) complexes, *Journal of the American Chemical Society*, **117**: 7562-7563.
4. C. Bubert, J. Blacker, S. M. Brown, J. Crosby, S. Fitzjohn, J. P. Muxworthy, T. Thorpe, J. M. J. Williams, (2001) Synthesis of water-soluble aminosulfonamide ligands and their application in enantioselective transfer hydrogenation, *Tetrahedron Letters*, **42**: 4037-4039.
5. Y. Arakawa, N. Haraguchi, S. Itsuno, (2006) Design of novel polymer-supported chiral catalyst for asymmetric transfer hydrogenation in water, *Tetrahedron Letters*, **47**: 3239-3243.
6. P. N. Liu, P. M. Gu, F. Wang, Y. Q. Tu, (2004) Efficient heterogeneous asymmetric transfer hydrogenation of ketones using highly recyclable and accessible silica-immobilized Ru-TsDPEN catalysts, *Organic Letters*, **6**: 169-172.
7. P. N. Liu, J. G. Deng, Y. Q. Tu, S. H. Wang, (2004) Highly efficient and recyclable heterogeneous asymmetric transfer hydrogenation of ketones in water, *Chemical Communications*, **18**: 2070-2071.
8. S. M. Sarkar, M. M. Yusoff, M. L. Rahman, (2015) Asymmetric transfer hydrogenation catalyzed by mesoporous MCM-41-supported chiral Ru-complex, *Journal of the Chinese Chemical Society*, **62**: 177-181.
9. J. Y. Jung, M. S. Sarkar, M. J. Jin, (2007) Heterogeneous asymmetric transfer hydrogenation with mesoporous silica SBA-15-supported Ru-TsCHDA catalyst, *Studies in Surface Science and Catalysis*, **165**: 693-696.
10. J. An, J. Zhao, G. Liu, T. Cheng, (2016) Fluorescence-marked mesoporous silica core-shell nanocatalyst for asymmetric transfer hydrogenation, *Sensors and Actuators B: Chemical*, **224**: 333-337.
11. O. Altan, M. K. Yilmaz, (2018) New phosphine-amino-alcohol tridentate ligands for ruthenium catalysed asymmetric transfer hydrogenation of ketone, *Journal of Organometallic Chemistry*, **861**: 252-262.
12. E. Breyse, C. Pinel, M. Lemaire, (1998) Use of heterogenized dialdimine ligands in asymmetric transfer hydrogenation, *Tetrahedron Asymmetry*, **9**: 897-900.
13. A. J. Sandee, D. G. Petra, J. N. Reek, P. C. Kamer, P. W. van Leeuwen, (2001) Solid-phase synthesis of homogeneous ruthenium catalysts on silica for the continuous asymmetric transfer hydrogenation reaction, *Chemistry: A European Journal*, **7**: 1202-1208.
14. S. Parambadath, A. P. Singh, (2009) Ru(II)-Chiral (1R,2S)-(+)-*cis*-1-amino-2-indanol immobilized over SBA-15 for asymmetric

- transfer hydrogenation reaction of prochiral ketones, *Catalysis Today*, **141**: 161-167.
15. Q. Yao, Z. H. Lu, K. Yang, X. Chen, M. Zhu, (2015) Ruthenium nanoparticles confined in SBA-15 as highly efficient catalyst for hydrolytic dehydrogenation of ammonia borane and hydrazine borane, *Scientific Reports*, **5**: 15186.
 16. L. W. Zhu, J. G. Wang, P. P. Zhao, F. Song, X. Y. Sun, L. H. Wang, H. Y. Cui, W. M. Yi, (2017) Preparation of the Nb-P/SBA-15 catalyst and its performance in the dehydration of fructose to 5-hydroxymethylfurfural, *Journal of Fuel Chemistry and Technology*, **45(6)**: 651-659.
 17. G. Liu, M. Yao, F. Zhang, Y. Gao, H. Li, (2008) Facile synthesis of a mesoporous silica-supported catalyst for Ru-catalyzed transfer hydrogenation of ketones, *Chemical Communications*, **3**: 347-349.
 18. Z. D. Eren, S. Tuncer, G. Gezer, L. T. Yildirim, S. Benerjee, A. Yilmaz, (2016) Improved solubility of celecoxib by inclusion in SBA-15 mesoporous silica: Drug loading in different solvents and release, *Microporous and Mesoporous Materials*, **235**: 211-223.
 19. S. Y. Kim, S. Parambadath, S. S. Park, C. S. Ha, (2017) Melamine-sulfonic acid functionalized SBA-15 for selective adsorption of metal ions from artificial seawater and wastewater, *Journal of Nanoscience and Nanotechnology*, **17(10)**: 7565-7574.
 20. K. M. Rao, S. Parambadath, A. Kumar, C. S. Ha, S. S. Han, (2018) Tunable intracellular degradable periodic mesoporous organosilica hybrid nanoparticles for doxorubicin drug delivery in cancer cells, *ACS Biomaterials Science and Technology*, **4(1)**: 175-183.
 21. X. S. Zhao, G. Q. Lu, (1998) Modification of MCM-41 by surface silylation with trimethylchlorosilane and adsorption study, *The Journal of Physical Chemistry B*, **102**: 1556-1561.
 22. (a) R. J. Staniewicz, R. F. Sympton, D. G. Hendrick, (1977) Preparation and investigation of the spectral and electrochemical properties of mixed-ligand ruthenium(II) complexes containing 1,8-naphthyridines, *Inorganic Chemistry*, **16**, 2166-2171. (b) F. Felix, J. Ferguson, H. U. Guedel, A. Ludi, (1980) The electronic spectrum of Tris(2,2'-bipyridine)ruthenium(2+), *Journal of American Chemical Society*, **102(12)**: 4096-4102.
 23. A. Mathew, S. Parambadath, S. S. Park, C. S. Ha, (2014) Hydrophobically modified spherical MCM-41 as nanovalve system for controlled drug delivery, *Microporous and Mesoporous Materials*, **200**: 124-131.
 24. K. Kosuge, T. Sato, N. Kikukawa, M. Takemori, (2004) Morphological control of rod- and fiberlike SBA-15 type mesoporous silica using water-soluble sodium silicate, *Chemistry of Materials*, **16**: 899-905.
 25. J. Canivet, G. Süss-Fink, (2007) Water-soluble arene ruthenium catalysts containing sulfonated diamine ligands for asymmetric transfer hydrogenation of α -aryl ketones and imines in aqueous solution, *Green Chemistry*, **9**: 391-397.
 26. S. Stephanie, J. P. Timothy, W. Charlotte, S. M. Benjamin, (2022) Tethered ruthenium(II) η^6 -arene complexes: Assessing the potential of benzylic substituents to control metal-centred chirality, and applications in asymmetric transfer hydrogenations of ketones, *Journal of Organometallic Chemistry*, **960**: 122232.
 27. P. A. Dub, N. V. Tkachenko, V. K. Vyas, M. Wills, J. S. Smith, S. Tretiak, (2021) Enantioselectivity in the noyori-ikariya asymmetric transfer hydrogenation of ketones, *Organometallics*, **40(9)**: 1402-1410.
 28. D. He, X. Xu, Y. Lu, M. J. Zhou, X. Xing, (2020) Asymmetric transfer hydrogenation of densely functionalized diheteroaryl and diaryl ketones by a Ru-catalyst of minimal stereogenicity, *Organic Letters*, **22(21)**: 8458-8463.
 29. L. L. Lou, S. Li, H. Du, J. Zhang, W. Yu, K. Yu, S. Liu, (2016) Short-mesochannel SBA-15-supported chiral 9-amino epincinchonine for asymmetric transfer hydrogenation of aromatic ketones, *ChemCatChem: The European Society Journal for Catalysis*, **8(6)**: 1199-1207.
 30. J. Lakshmidevi, V. Vakati, B. R. Naidu, M. Raghavender, K. S. V. Krishna Rao, K. Venkateswarlu, (2021) Pd (5%)-KIT-6, Pd (5%)-SBA-15 and Pd (5%)-SBA-16 catalysts in water extract of pomegranate ash: A case study in heterogenization of Suzuki-Miyaura reaction under external base and ligand free conditions, *Sustainable Chemistry and Pharmacy*, **19**: 100371.
 31. K. S. V. K. Rao, K. Nagaraja, B. Adilakshmi, J. Lakshmidevi, G. V. Reddy, S. S. Han, K.M. Rao, (2022) Recent advances in chitosan-based composite materials in organic transformations-a review, *Current Organic Chemistry*, **26(13)**: 1294-1302.
 32. G. Venkatesulu, P. K. Babu, Y. Maruthi, C. Madhavi, A. Parandhama, M. C. Subha, K. C. Rao, (2016) Design and application of H-ZSM-5 zeolite loaded hydroxy propyl cellulose/poly (vinyl pyrrolidone) mixed matrix membranes for dehydration of ethanol by pervaporation, *Indian Journal of Advances in Chemical Science*, **4(4)**: 496-505.

*Bibliographical Sketch



Dr. Surendran Parambadath, working as Assistant Professor in Chemistry at Sree Neelakanta Government Sanskrit College, Pattambi, Kerala, India. He had B.Sc, B.Ed, M.Sc, and M.Phil from University of Calicut, Kerala. He had M.Tech (Industrial Catalysis) from Cochin University of Science and Technology (CUSAT). He did Ph.D work under the guidance of Dr. Anand Pal Singh, in Catalysis at National Chemical Laboratory, Pune-India. He did post-doctoral research at department of Polymer Science and Engineering, Pusan National University, South Korea under the supervision of Prof. Dr. Chang Sik-Ha. He has published 34 papers in well reputed national and international journals. He has attended and presented research works in National and International conferences and seminars. He has 12 years teaching experience in college level.



Dr. Aneesh Mathew is an Assistant Professor at Government Engineering College in Idukki, India, in the department of Basic Science. He earned his Ph.D degree from the department of polymer science and engineering at Pusan National University in the Republic of Korea is where. Later, he served as a Research Professor at the Research of Reaction and Separation Nanomaterials Laboratory (RSNL), Chungnam National University, Republic of Korea, where he focused on zeolite for separation applications. Following his brief stay at the Korean Institute of Science and Technology (KIST), he began working as an Assistant Professor in the chemistry department at Marian College and Pavanatma College, both of which are close to his hometown. He was a Senior Executive at Torque Pharma, a well-known pharmaceutical business, prior to his current role. He filed one US patent and has 15 SCI articles and two conference publications to his credit.